Int. j. adv. multidisc. res. stud. 2024; 4(2):1060-1064

Received: 23-02-2024
Accepted: 03-04-2024

International Journal of Advanced Multidisciplinary Research and Studies

ISSN: 2583-049X

Study the Effect of Ni Doping on Structural, Optical and Electrical Properties of $Ni_{1-x}Ag_xO$ Thin Films Deposited by Spray Pyrolysis Technique

[1] C Zaouche, [2] S Khelaifa

[1] Higher School of Saharan Agriculture - El Oued, PB 90 Chouhada, El Oued 39011, Algeria

[2] Department of Physics, Faculty of Exact Sciences, University Elchahid Hamma Lakhder, 39000 El Oued, Algeria

DOI: https://doi.org/10.62225/2583049X.2024.4.2.2622

Corresponding Author: **C Zaouche**

Abstract

The effect of Ag doping on optical, structural and electrical properties of deposited $Ni_{1-x}Ag_xO$ thin films on glass substrate by spray pyrolysis technique has been studied. The main objective of this research is to study the change of the physical and optical properties of $Ni_{1-x}Ag_xO$ thin films that are fabricant to semiconductor with different doping levels x. These levels are 0 at.%, 2 at.%, 4 at.%, 8 at.% and 10 at.%. The transmission spectra show that the $Ni_{1-x}Ag_xO$ thin films have a good optical transparency in the visible region from 68 to 83%. The optical gap energy of the $Ni_{1-x}Ag_xO$ thin films varied between 3.70 and 3.81 eV. The urbach energy varied between 245 and 289 meV. However, the $Ni_{0.96}Zn_{0.04}O$ thin films have many defects with maximum value of urbach energy. The $Ni_{0.96}Ag_{0.04}O$ thin films have minimum value of optical gap energy. The $Ni_{0.96}Ag_{0.04}O$ thin films have maximum value of the electrical conductivity which is 0.023 $(\Omega.cm)^{-1}$. The $Ni_{0.92}Ag_{0.08}O$ thin films have maximum value of the transmission which is 83%. The average electrical conductivity of our films is about (0.0184 $(\Omega.cm)^{-1}$). XRD patterns of the $Ni_{1-x}Ag_xO$ thin films indicate that films are polycrystalline with cubic structure.

Keywords: Nickel Oxide, Thin Films, Spray Pyrolysis, Optical Gap Energy, Urbach Energy, The Electrical Conductivity

1. Introduction

Nickel oxide is one of the most important semiconductor materials in the environmental field due to the detecting ability of toxic gases [1]. Nickel oxide (NiO) has a several different applications in the field of pizoelectronic, optoelectronic, environmental and renewable energy such as sensors, fuel cell electrodes, catalysis, thermoelectric devices, dye-sensitized solar cells (DSSCs) and electrochromic material for displays [2-8]. Moreover, it is used to find suitable material with enhanced properties for gas sensing applications for detecting the sensibility in the environment such as NOx, SOx, CO, CO_2…, at high temperature. Because of its semiconductor nature with controlling optical transparency and electrical conductivity, finding the form of the applied interaction is significant. However, several studies have been made to find that the NiO have a high optical transparency and good electrical conductivity at various experimental conditions. NiO thin films have a direct band gap ranging from 3.5 to 4.3 eV [9-10].

Nickel oxide is used as thin layers, which can be deposited in several methods, including molecular beam epitaxy (MBE), electrochemical deposition, pulsed laser deposition (PLD), chemical vapor deposition and spray Sol–Gel methods, spray pyrolysis technique [11-17]. We used the argent doped NiO thin films to improve the optical and electrical properties of deposited thin films. This is a metal transition in the periodic table, which was used in the research because of some rare earth material quality due to the increase in the optical band gap energy (broadening).

In this work, we have prepared Ag doped NiO thin films by using the spray pyrolysis technique deposition on glass substrate which its temperature is 480 °C. We sprayed this glass substrate for 5 minutes. Ag doped NiO thin films were synthesized with different doping levels (0, 2, 4, 8 and 10 at. %) for $Ni_{1-x}Ag_xO$. The $Ni_{1-x}Ag_xO$ thin films were used to enhance the optical and electrical properties of deposited thin films. However, we have studied the change of the optical, structural and electrical properties of $Ni_{1-x}Ag_xO$ thin films that are fabricant to semiconductor.

2. Experimental procedure

$Ni_{1-x}Ag_xO$ solutions were prepared by dissolving the nickel acetate ($Ni(CH_3.CO_2)_2.4H_2O$) andargent acetate ($AgC_2H_3O_2$) with 0.5 mol l^{-1}. In this work, we have used a Ag doping with various concentrations in the game Ag/Ni = 0, 2, 4, 8 and 10 at.% or (x = 0, 0.02, 0.04, 0.08 and 0.10). Then, we have added a drop of HCl to stabilize heating solution. The mixture solution was stirred at room temperature and heated at 40 °C for 2 h to yield a clear and transparent solution. The coating was made 1 day after the precursor was prepared.

The $Ni_{1-x}Ag_xO$ samples were prepared by spraying the coating solution onto glass substrate. Its temperature is 480 °C for 5 minutes to obtain a thin film. The prepared $Ni_{1-x}Ag_xO$ thin films at different Ag doping levels are 0 at.%, 2 at.%, 4 at.%, 8 at.% and 10 at.%. After the deposition of the thin layers, we left substrate to decrease its temperature to the one of the room.

The structural properties of $Ni_{1-x}Ag_xO$ thin films were studied by means of X-ray diffraction (XRD Bruker AXS-8D) with CuKa radiation (λ=0.15406 nm) in the scanning range of (1h) which was between 20° and 70°. The optical transmission of the deposited films was measured in the range of (300–900nm) by using an ultraviolet-visible spectrophotometer (LAMBDA 25) and the electrical conductivityσ was measured by four-point methods.

3. Results and discussion

3.1 Structural properties of $Ni_{1-x}Ag_xO$ thin films

The structural characterization of the $Ni_{1-x}Ag_xO$ thin films is carried out by X-ray diffraction method that is shown in Fig 1. XRD spectra indicate that the films exhibit polycrystalline structure that belongs to the cubic type of NiO (JCPDS) No. 73-1519) [18]. Fig 1 shows that the XRD peaks at 37.4064° and 43.2092° corresponding to (111) and (200) crystal planes respectively, the peaks position was accordant with Abdur Rahman *et al.* [19]. We observed that the intensity of (111) and (002) peaks increase in thin films with the increasing doping levels x at x=0.10. This information confirmed that the preferred orientation is along to (111) and (002) planes. However, the film at x=0.10 has higher and sharper diffraction peaks indicating an enhancement of crystallinity with comparison to other films.

The structure information was defined by the diffraction peak angles of the Ag doped NiO thin films (see Table 1). The lattice parameter **a** of Ag doped NiO thin films was calculated from XRD patterns by using the following equation [20]:

$$\frac{1}{d_{hkl}^2} = \frac{h^2 + k^2 + l^2}{a^2} \quad (1)$$

Where **h**, **k** and **l** are the Miller indices of the planes. **a** is the lattice parameter and $\mathbf{d_{hkl}}$ is the inter planar spacing. The crystallite sizes **G** of (111) and (200) planes were calculated according to the Scherer equation [21-22]:

$$G = \frac{0.9\lambda}{\beta \cos\theta} \quad (2)$$

Where **G** is the crystallite size, $\boldsymbol{\beta_{1/2}}$ is the full width at half-maximum (FWHM), **θ** is Bragg angle of the diffraction peaks and **λ** is the X-ray wavelength (λ=0.15406 nm). The variations are shown in Tables 1 and 2. The $Ni_{0.96}Ag_{0.04}O$ thin films have minimum value of the crystallite size which is 8.742987 nm of (111) peak and 10.658580 nm of (200) peak.

The variations of the crystallite size and diffraction angle according to (111) and (200) peaks presented in Fig 2 a and b shows the variation of crystallite size and diffraction angle of Ag doped NiO thin films as a function of Ag doping level. In Fig 2a, we have observed that the diffraction angles of (111) plan decreased with increasing doping levels x from 0.04 to 0.10 (see Tables 1). The crystallite size of (111) plan decreased to minimum value obtained at x=0.04 (see Tables 1). On the other hand, fig 2b shows that the diffraction angles of (200) plan decreased then increased and decreased again with increasing doping levels x to reach the maximum value obtained at x=0.10 (see Table 2). But we observed that the crystallite size of (200) plan decreased to minimum value at x=0.04. The decrease of the crystallite size has been indicated by the enhancement of the crystallinity and a-axis orientation of Ag doped NiO thin films. These phenomena were observed in [23-27]. This result can be explained by coalescence of the crystallite of the thin films to improve oxygen diffusion [28]. The $Ni_{0.96}Ag_{0.04}O$ thin films have best structural properties.

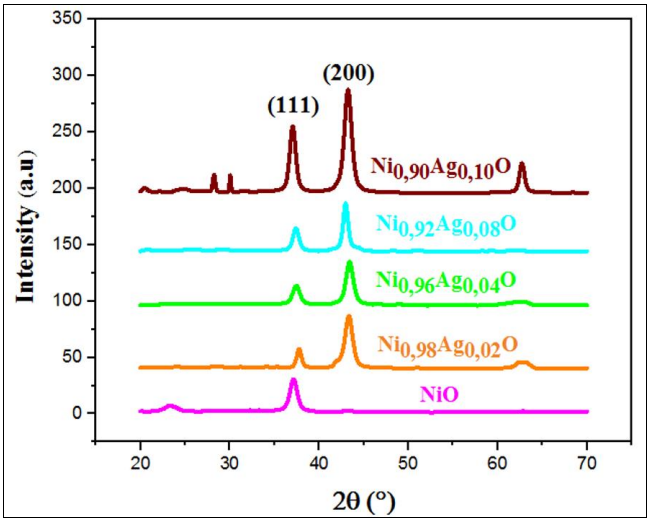

Fig 1: X-ray diffraction of $Ni_{1-x}Ag_xO$ thin films as a function of Ag doping level

Table 1: The structural parameters of $Ni_{1-x}Ag_xO$ thin film as a function of Ag doping level of (111) diffraction peak

X	2θ(°)	d (nm)	$\beta_{1/2}$ (°)	G(nm)	a(nm)
0	37.4536	0,240044	0.4091	20.513691	0,415769
0.02	37.4136	0,240292	0.6453	13.003501	0,416197
0.04	37.5338	0,239550	0.9601	8.742987	0,414912
0.08	37.4517	0,240056	0.8027	10.454844	0,415789
0.10	37.1792	0,241753	0.6453	12.994537	0,418728

Table 2: The structural parameters of $Ni_{1-x}Ag_xO$ thin film as a function of Ag doping level of (200) diffraction peak

x	2θ(°)	d (nm)	$\beta_{1/2}$ (°)	G(nm)	a(nm)
0	43.0222	0,210175	0.3304	25.855795	0,420350
0.02	43.0208	0,210181	0.4878	17.512738	0,420363
0.04	43.4585	0,208165	0.8027	10.658580	0,416333
0.08	43.0594	0,210002	0.6453	13.240116	0,420004
0.10	43.4853	0,208043	0.2517	33.994592	0,416086

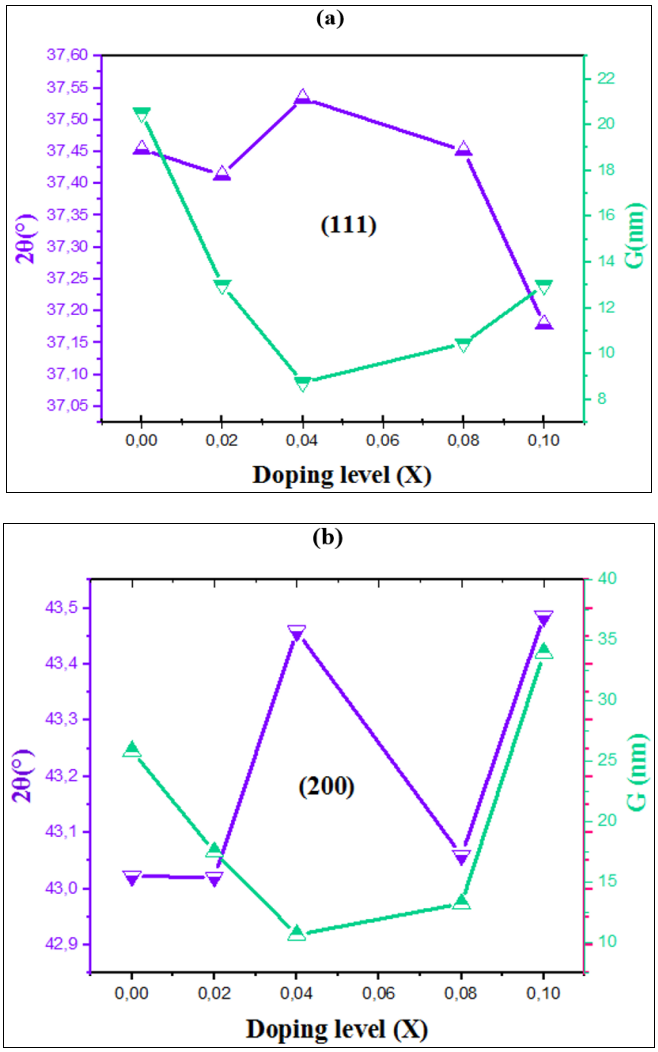

Fig 2: The variation of crystallite size and diffraction angle of Ag doped NiO thin films according to a (111) phase and b (200)

3.2 Optical properties of $Ni_{1-x}Ag_xO$ thin films

The Optical characterizations of fabricated $Ni_{1-x}Ag_xO$ thin films by doping levels x were performed by measuring the transmittance and absorbance in the wavelength region 300 to 900 nm as it is shown in Figure 3 and 4. As we can see, the value of the average transmission of spray $Ni_{1-x}Zn_xO$ thin films is about 73% in the visible region. But for these doping levels x, the region of the absorption edge was located between 315 and 365 nm in comparison with others which are found at 355 and 370 nm [29-30]. It is related region between of the valence band and the conduction band. Fig 4 presents the variation of absorbance data of thin films of $Ni_{1-x}Ag_xO$. The absorption edge shifts was observed clearly at wavelength shorter than 370nm. The absorption edge shifts of $Ni_{1-x}Ag_xO$ thin films increased with the increase of doping levels x. As we can note, the optical property of thin films of $Ni_{1-x}Ag_xO$ is affected by doping levels x.

The role of doping levels x on the transmission of thin films of $Ni_{1-x}Ag_xO$ was clearly observed on the thin films quality due to the higher transparency. The high transparency was obtained in Ag doped NiO thin film with at 8% due to the interstitial site of Ag and Ni. The $Ni_{0.92}Ag_{0.08}O$ thin films have best transmission. That absorbance and the optical band gap energy E_g of fabricated $Ni_{1-x}Ag_xO$ thin films were determined by the following relations [31-33]:

$$A = \alpha d = -\ln T \quad (3)$$

$$(Ahv)^2 = C\left(hv - E_g\right) \quad (4)$$

where **A** is the absorbance of fabricated $Ni_{1-x}Ag_xO$ thin films, **α** is the absorption coefficient, **d** is the film thickness, **T** is the transmission of fabricated $Ni_{1-x}Ag_xO$ thin films, **C** is a constant, **hυ** is the energy of photon $\left(h\upsilon = \frac{1240}{\lambda(nm)}\ (eV)\right)$ and $\mathbf{E_g}$ is the band gap energy of the semiconductor. However, the disorder or Urbach energy ($\mathbf{E_u}$) also was determined by the expression follow [34-35]:

$$A = A_0 \exp\left(\frac{hv}{E_u}\right) \quad (5)$$

Where $\mathbf{A_0}$ is a constant, **hυ** is the energy of photon and $\mathbf{E_u}$ is the Urach energy, the tail width of the Urbach energy was used to characterize the order of the defects. The variation of optical band gap energy and Urbach energy of fabricated $Ni_{1-x}Ag_xO$ thin films as a function of doping levels x are presented in the Fig 5. The band gap energy was observed a smaller than 3.82 eV. The value of band gap energy decreased and increased with the increase in doping levels from. 3.70 to 3.81 eV. The diminution in the optical band gap energy value of $Ni_{1-x}Ag_xO$ thin films can be illustrated by the effect of quantum confinement due to the diminution in the crystallite size of fabricated $Ni_{1-x}Ag_xO$ thin films (see Fig 2). As can be seen in Fig 5, that the value of Urbach energy increased and decreased with the increase in doping levels from 245 to 289 meV. Also, this can be related by the diminution of the crystallite size value (see Fig 2). The $Ni_{0.96}Ag_{0.04}O$ thin films have best optical properties.

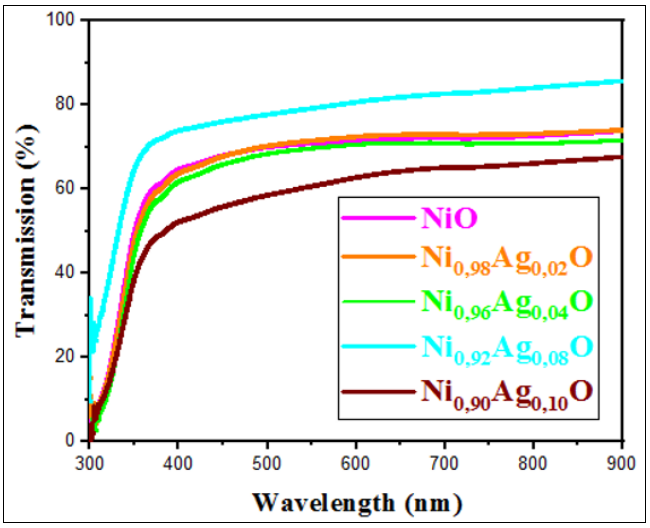

Fig 3: Transmission spectra of $Ni_{1-x}Ag_xO$ thin films as a function of Ag doping level

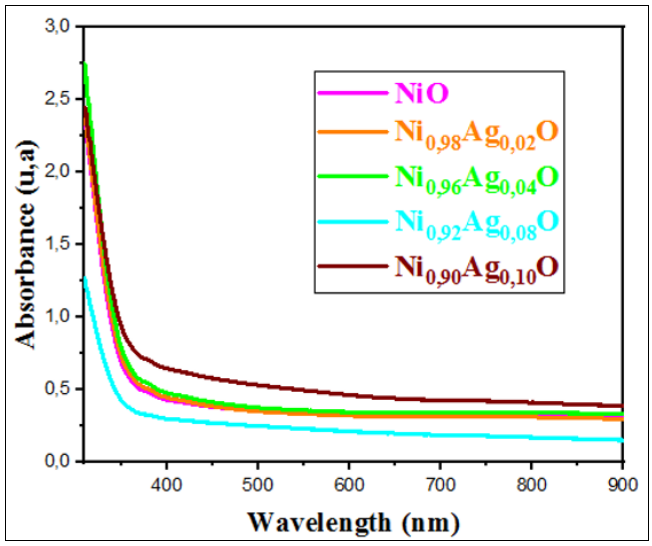

Fig 4: Absorbance spectra of $Ni_{1-x}Ag_xO$ thin films as a function of Ag doping level

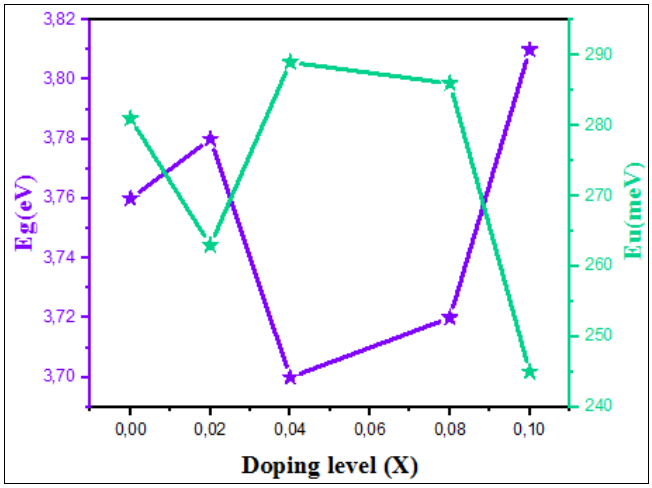

Fig 5: The variations of optical pand gap energy and Urbach energy of Ag doped NiO thin films at various doping levels

3.3 Electrical properties of $Ni_{1-x}Ag_xO$ thin films

The four-points probe method was used to determine the electrical conductivity of $Ni_{1-x}Ag_xO$ thin films, it is based on measuring the sheet resistance of the films as expressed by [36]:

$$R_{sh} = \frac{\pi}{\ln(2)} \cdot \frac{V}{I} \quad (6)$$

Where **I** is the applied currant I=1 nA and **V** is the measurement voltage. However, the electrical conductivity **σ** is also determined by the following equation [37]:

$$\sigma = \frac{1}{d.R_{sh}} \quad (7)$$

Fig 6 shows the variation of the electrical conductivity of Ag doped NiO thin films as a function of Ag doping level. As can be seen, the electrical conductivity increases with increasing the Ag doping level up to 4 at.% where we obtained a maximum conductivity value which was 0.0023 $(\Omega.cm)^{-1}$. The increase in the conductivity of the $Ni_{1-x}Ag_xO$ thin films can be explained by the displacement of the electrons. The latter comes from the Ag^+ donor ions in the substitutional sites of Ni^{+2} and the formation of the molecular $NiAg_2O$ existed on the surface. The increase in the conductivity of deposited films after 4 at.% can be related to the increase of the potential barriers, because the introduced atoms are segregated into the grain boundaries [38-39]. The $Ni_{0.96}Ag_{0.04}O$ thin films have best electrical properties. The Figures (2, 5 and 6) showed the decrease in the crystallite size, the decrease in optical gab energy, the increase in urbach energy and the increase in electrical conductivity. These results explain the good crystallization of the thin films according to [40, 41, 42, 43].

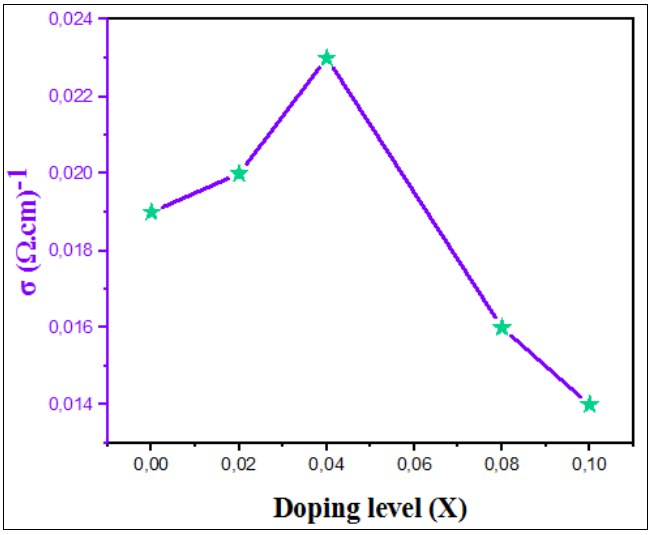

Fig 6: The electrical conductivity variation of $Ni_{1-x}Ag_xO$ thin films as a function of Ag doping level

4. Conclusion

In this work, nickel acetate and argent acetate were used in spray pyrolysis to successfully deposit argent-doped nickel oxide thin films (Ag/Ni = 0, 2, 4, 8, and 10 at. %) on glass substrates. In the visible spectrum, the $Ni_{1-x}Ag_xO$ thin films exhibit transparency. The energy of the optical gap varies from 3.70 to 3.81eV. The Urbach energy fluctuates between 245 and 289meV. That being said, $Ni_{0.96}Ag_{0.04}O$ thin films show many flaws at the maximal Urbach energy. Thin films of $Ni_{0.96}Ag_{0.04}O$ have the lowest optical gap energy. The $Ni_{0.96}Ag_{0.04}O$ thin films also exhibited the highest electrical conductivity. The crystallite sizes of the $Ni_{0.96}Ag_{0.04}O$ films range from 8.742987 nm (111) at the minimum to 10.658580 nm (200) at the peak. The XRD patterns of the $Ni_{1-x}Ag_xO$ thin films indicate that the films are polycrystalline with a cubic structure. The electrical conductivity of the deposited films is on the order of 0.0184 $(\Omega.cm)^{-1}$. The $Ni_{0.96}Ag_{0.04}O$ thin films have best structural, optical and electrical properties. The $Ni_{0.92}Ag_{0.08}O$ thin films have best transmission. Figures 2, 5, and 6 show the decrease in the crystallite size, the decrease in the optical gap energy, the increase in the Urbach energy, and the increase in the electrical conductivity. These results explain the good crystallization of the thin films.

5. References

1. Verma V, Katiyar M. Thin Solid Films. 2013; 527:369.
2. Chen SC, Kuo TY, Lin YC, Lin HC. Thin Solid Films. 2011; 519(15):4944.

3. Sharma R, Acharya AD, Shrivastava SB, Patidar MM, Gangrade M, Shripathi T, *et al*. Optik. 2016; 127(11):4661.
4. Benramache S, Aouassa M. Journal of Chemistry and Materials Research. 2016; 5(6):119.
5. Dendouga S, Benramache S, Lakel S. Journal of Chemistry and Materials Research. 2016; 5(4):78.
6. Dini D, Halpin Y, Vos JG, Gibson EA. Coordination Chemistry Reviews. 2015; 304-305:179.
7. Cai GF, Gu CD, Zhang J, Liu PC, Wang XL, You YH, *et al*. Electrochimica Acta. 2013; 87:341.
8. Nwanya AC, Offiah SUI, Amaechi C, Agbo S, Ezugwu SC, Sone BT, *et al*. Electrochimica Acta. 2015; 171:128.
9. Romero R, Martin F, Ramos-Barrado JR, Leinen D. Thin Solid Films. 2010; 518(16):4499.
10. Chtouki T, Soumahoro L, Kulyk B, Bougharraf H, Kabouchi B, Erguig H, *et al*. Optik. 2017; 128:8.
11. Deokate RJ, Kalubarme RS, Park CJ, Lokhande CD. 2017; 224:378.
12. Yu Y, Li X, Shen Z, Zhang X, Liu P, Gao Y, *et al*. Journal of Colloid and Interface Science. 2017; 490:380.
13. Offiah SU, Nwodo MO, Nwanya AC, Ezugwu SC, Agbo SN, Ugwuoke PU, *et al*. Optik. 2014; 125:2905.
14. Chen SC, Kuo TY, Lin YC, Hsu SW, Lin HC. Thin Solid Films. 2013; 549:50.
15. Xia XH, Tu JP, Zhang J, Wang XL, Zhang WK, Huang H. Electrochimica Acta. 2008; 53(18):5721.
16. Castro-Hurtado I, Herra´n J, Mandayo GG, Castan˜o E. Thin Solid Films. 2011; 520(3):947.
17. Zaouche C, Aoun Y, Benramache S, Gahtar A. Scientific Bulletin of valahia University materials and mechanics. 2019; 17(17):27.
18. Cao J, Wang Z, Wang R, Liu S, Fei T, Wanga L, *et al*. Materials Chemistry A. 2015; 3(10):5635.
19. AbdurRahman M, Radhakrishnan R, Gopalakrishnan R. Alloys and Compounds. 2018; 742:421.
20. Saleh AF. Application or Innovation in Engineering & Management. 2013; 2(1):16.
21. Gahtar A, Benramache S, Ammari A, Boukhachem A, Ziouche A. Inorganic and Nano-Metal Chemistry. 2022; 52(1):112.
22. Gahtar A, Zaouche C, Ammari A, Dahbi L. Chalcogenide Letters. 2023; 20(5):377.
23. Beji N, Reghima M, Souli M, Turki NK. Alloys and Compounds. 2016; 675:231.
24. Chatterjee S, Saha SK, Pal AJ. Solar Energy Materials and Solar. 2016; 147:17.
25. Garcia-Garcia FJ, Salazar P, Yubero F, González-Elipe AR. Electrochimica Acta. 2016; 201:38.
26. Ali N, Hussain A, Ahmed R, Wang MK, Zhao C, UlHaq B, *et al*. Renewable and Sustainable Energy Reviews. 2016; 59:726.
27. Dahbi L, Zaouche C, Benkrima Y, Gahtar A. Tobacco Regulatory Science. 2023; 9(1)2819.
28. Benramache S, Benhaoua B. Superlattices and Microstructures. 2012; 52(16):1062.
29. Bayram O, Sener E, İgman E. Simsek O. Journal of Materials Science Materials in Electronics. 2019; 30:3452.
30. Zaouche C, Benramache S. International Journal of Advanced Multidisciplinary Research and Studies. 2023; 3(5):68.
31. Diha A, Benramache S, Benhaoua B. Optik. 2018; 172:832.
32. Benramache S, Aoun Y, Lakel S, Mourghade H, Gacem R, Benhaoua B. Journal of Nano- and Electronic Physics. 2018; 10:06032.
33. Zaouche C, Dahbi L, Benramache S, Harouache A, Derouiche Y, Kharroubi M, *et al*. Journal of Ovonic Research. 2023; 19(2):197.
34. Daranfed W, Aida MS, Hafdallah A, Lekiket H. Thin Solid Films. 2009; 518:1082.
35. Gahtar A, Benramache S, Zaouche C, Boukacham A, Sayah A. Advances in Materials Science. 2020; 20(3):36.
36. Benramache S, Benhaoua B, Chabane F. Journal of Semiconductors. 2012; 33(9):093001.
37. Dahbi L, Zaouche C, Gahtar A, Magni C, Seggai S. Neuroquantology. 2023; 21(7):883.
38. Magni C, Zaouche C, Dahbi L, Seggai S, Guedda E. Digest Journal of Nanomaterials and Biostructures, 2024; 19(1):359.
39. Zaouche C, Benramache S, Gahtar A. Biomedical Journal of Scientific Technical Research. 2023; 52(3):43761.
40. Zaouche C, Gahtar A, Benramache S, Derouiche Y, Kharroubi M, Belbel A, *et al*. Digest Journal of Nanomaterials and Biostructures. 2022; 17(4):1453.
41. Benramache S, Aoun Y, Charef A, Benhaoua B, Lake S. Inorganic and Nano-Metal Chemistry. 2019; 49:177.
42. Othmane M, Attaf A, Saidi H, Bouaichi F, Lehraki N, Nouadji M, *et al*. International Journal of Nanoscience. 2015; 15:1650007.
43. Gahtar A, Benali A, Benramache S, Zaouche C. Chalcogenide Letters. 2022; 19(2):103.